1

An Introduction to Chalcogenide Glasses

1.1 Introduction

Chalcogenide glasses are based on the chalcogen elements S, Se, and Te. These glasses are formed by the addition of other elements such as Ge, As, Sb, Ga, etc. They are low-phonon-energy materials and are generally transparent from the visible up to the infrared. Chalcogenide glasses can be doped by rare-earth elements, such as Er, Nd, Pr, etc., and hence numerous applications of active optical devices have been proposed. Since chalcogenide-glass fibers transmit in the IR, there are numerous potential applications in the civil, medical, and military areas. Passive applications utilize chalcogenide fibers as a light conduit from one location to another point without changing the optical properties, other than those due to scattering, absorption, and reflection.

These glasses are optically highly nonlinear and could therefore be useful for all-optical switching (AOS). Chalcogenide glasses are sensitive to the absorption of electromagnetic radiation and show a variety of photoinduced effects as a result of illumination. Various models have been put forward to explain these effects, which can be used to fabricate diffractive, waveguide and fiber structures. For recent reviews, see [1–4]. Next-generation devices for telecommunication and related applications will rely on the development of materials which possess optimized physical properties that are compatible with packaging requirements for systems in planar or fiber form. This allows suitable integration to existing fiber-based applications, and hence requires appropriate consideration as to material choice, stability, and long-term aging behavior.

1.2 Structure of Chalcogenide Glasses

Solids are a particular state of condensed matter characterized by strong interactions between the constituent particles (atoms, molecules). Solids can be found or prepared either in an ordered (crystalline) state or in a disordered (noncrystalline) state. While the ordered state of a solid is limited to only

a few structural forms, a disordered material is neither unique nor clearly defined. An ideal crystal corresponds to a regular arrangement of atoms in a lattice with well-defined symmetry, and a structural unit called the unit cell can be defined. Translation of the unit cell along the three coordinate axes reproduces the whole assembly of atoms. A real crystal does not exhibit perfect periodicity in space and contains various kinds of imperfections or defects. Solids which lack the periodicity of the atoms are called noncrystalline solids or amorphous, vitreous or glassy solids. While crystals possess long-range order (LRO), in amorphous materials short-range order (SRO) still exists. Although the first and second nearest-neighbor coordination shells are well-defined, atoms in the third coordination sphere start to become uncorrelated with those in the first one. In other words, the limit of short- and medium-range order is the first 3–4 interatomic distances. The price to be paid for the loss of LRO is the appearance of fluctuations in angles and distances between the bonds. The ideal noncrystalline network is difficult to define. Particularly, different thermal treatments lead to various noncrystalline arrangements of atoms. A continuous random network [5] might be considered to be an ideal noncrystalline network for covalent solids.

The structure of chalcogenide glasses, however, cannot be described by means of a continuous random network which is isotropic in three dimensions, as in the case of amorphous silicon for example. As_2S_3, As_2Se_3, GeS_2, and $GeSe_2$ can be locally layer-like, while pure S and Se are chain like. For all these materials, there is considerable flexibility of the structure as a result of the weak van der Waal's bonding between layers or chains [6], so that changes in the structure can be relatively easily accommodated.

Raman (or inelastic) scattering of light in a material yields structural and dynamic information on a molecular level. The nondestructive nature of the probe, and flexibility in sampling arrangements, has opened up many potentially new areas where Raman measurements have proven valuable [7,8]. Near-infrared (NIR) Raman spectroscopy can be used in the analysis of materials which are strongly absorbing in the visible. A distinct advantage over the more conventional approach using the visible part of the spectrum as the excitation wavelength is the ability to obtain the Raman spectrum of photosensitive compounds without interference from photoreactions caused by the probe beam. In As–S–Se chalcogenide glasses, shifting the excitation wavelength to 840 nm (typically below the band gap) allows one to obtain high-quality Raman spectra without material modification. Raman spectroscopy can be extremely powerful in the microstructural analysis of single and multilayer waveguide devices [9]. Here, the material of interest is made in the form of a slab waveguide, thereby significantly increasing both the scattering volume and the electric-field intensity within the film. Raman scattering in the NIR can be excited with 840 nm radiation from a tunable Ti:sapphire laser (30–50 mW). The dominant feature in binary sulfide and selenide compounds are bands at 345 cm^{-1}($As_{40}S_{60}$) and 230 cm^{-1} ($As_{40}Se_{60}$), respectively, [10] (see Fig. 1.1).

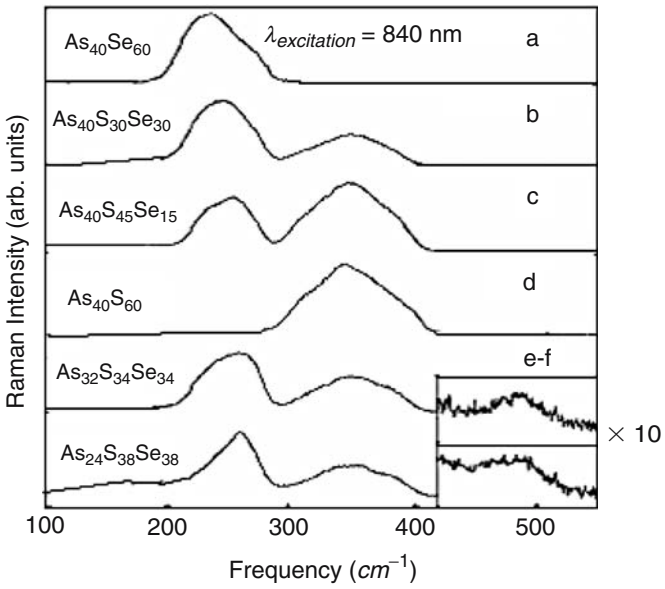

Fig. 1.1. Raman spectra of bulk glasses obtained with near-infrared excitation ($\lambda = 840\,\text{nm}$) as a function of compositional variation. Spectral resolution is $1.5\,\text{cm}^{-1}$ (after [10])

A strong broad band is seen which is attributed to the antisymmetric As–(S,Se)–As stretching vibration in $As(S, Se)_3$ pyramidal units. In ternary compounds with a S/Se = 1 molecular ratio and decreasing As content, a progressive decrease in the intensity of these broad bands is observed, indicative of a decrease in the number of As-containing pyramidal sites. New bands appearing around $255\,\text{cm}^{-1}$ and 440–$480\,\text{cm}^{-1}$ form in chalcogen-rich glasses, and are attributed to Se–Se homopolar bonds. These units serve as chalcogen chains connecting the remaining pyramidal units. The small numbers of S–S bonds, indicated by a weak band near $495\,\text{cm}^{-1}$, for equal concentrations of S and Se suggests that S stays with the remaining pyramids and that it is the Se which dominates the connecting chain units. Deviations from bulk glass properties in fibers and films are observed. The extent of such compositional variation, and the resulting structural units formed, varies with the specific fiber or film-processing technique used. Neutron-scattering and X-ray diffraction studies on bulk sulfide and selenide glasses and their thin films [11] have shown variations in structural units on the intermediate-range order scale. Depending on processing conditions, polymeric cages (based on As_4S_4 units) or less connected groups of As–S pyramidal units, were observed. Furthermore, these units are much more metastable and can be structurally modified or eliminated with postdeposition processing. Waveguide Raman spectroscopy (WRS) has been applied to the structural characterization of chalcogenide

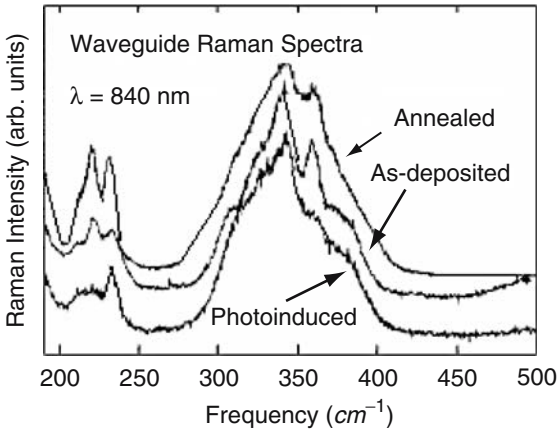

Fig. 1.2. Variation in waveguide Raman spectra for a fresh, annealed, and photostructurally modified As_2S_3 channel waveguide (exposure $\lambda = 514.5$ nm). Excitation wavelength was 840 nm (after [10])

glasses [12, 13]. The excitation beam (840 nm) was launched into the end face of an As_2S_3 channel waveguide at various lateral positions. Although the As_2S_3 film had a thickness of just 1.5 μm, the high signal-to-noise ratio achieved by guided-mode excitation was evident and low-frequency Raman peaks were well separated from interfering Rayleigh scattering. In comparison with the bulk, new substructures appeared in the film spectra as compared with the broad features of the bulk spectra (see Fig. 1.2).

These differences in the spectra from the bulk are due to different (molecular) arrangements of the constituent atoms within the films. These sharp, molecular-signature features were confirmed not to be due to crystallinity within the film, but most likely result from the formation of as-deposited As_4S_4 units [11, 14]. Rutherford backscattering spectroscopy (RBS) is an analytical tool that gives very useful information regarding compositional and structural analysis of films, as well as a precise measurement of the film thickness. Results obtained showed no apparent variation in composition and small (less than 10%) density variation in single-layer As_2S_3 films [15]. Multilayer films, whose thickness can be measured using SEM images, display compositional and density modifications associated with the annealing process. Film ageing was investigated in films after almost a year. Stoichiometric and thickness modifications, caused by ageing, were observed in unannealed structures [15]. No apparent changes were detected in annealed films. The RBS data shows that the ratio of the sulfur-to-arsenic concentration increases during the annealing process. This suggests that the sulfur is not evaporating during annealing. However, SEM shows a modification in the layer thickness for the multilayer structure. This result implies that the molecules in the films are rearranging. NIR Raman results complement this conclusion.

Chalcogenide glasses seem to experience slight modifications with time, under standard conditions (i.e. room temperature). However, these structural modifications or relaxation in the molecular structure of the films are less apparent in annealed structures, which suggests that annealed films are fairly stable in time. Seal et al. [16] have used X-ray photoelectron spectroscopy (XPS) to study the resulting chemical composition of As_2S_3 at the film surface as compared to the parent bulk glass and the corresponding variation in the nature of chemical bonds and electronic structure. Ar^+-ion sputtering converts the amorphous phase into a crystalline phase as the binding energy of the As peak increases from 42.7 to 43.8 eV [16]. Inference of the crystalline phase in the sputtered region is based on the fact that 99.99% pure melted As_2S_3 glass has a similar binding energy to that seen for As in its crystalline form. It was found that laser irradiation induces structural and chemical changes in the sample, as can be seen from the change in the As/S ratio with illumination. Polarization direction, vertical and circular polarization were found to induce an As-deficient structure and horizontal polarization was found to make the system As-rich [16]. It was also found that, when films are illuminated, some non-bridging S atoms were observed but no nonbridging atoms appeared to be created when the sample was sputtered with an Ar^+ beam [16]. EXAFS studies [17] have shown that there is chemical disorder in the structural network of GaLaS thin films, although chemical ordering is predominant in bulk GaLaS glass. EXAFS results show that gallium is always fourfold coordinated in the GLS network. Both Ga–Ga and S–S bonds occur in GLS thin-film samples but the lanthanum atoms remain eightfold coordinated by sulfur alone. The bond lengths were the same as those found in bulk glass. Although the nearest-neighbor environment is well-defined, there is considerable bond-angle variation, and hence a wide variation in second-neighbor distances. Benazeth et al. [18] also studied the structure of bulk GLS glasses using EXAFS at the gallium K edge and lanthanum L_3 edge. Their results show that gallium atoms in the glass exist in tetrahedral networks of GaS_4, and the Ga–S distances in the glasses are identical to those existing in the crystalline form of Ga_2S_3. The gallium and sulfur environment in crystalline Ga_2S_3 is such that two of the three sulfur atoms are linked to three gallium atoms and the third sulfur atom is linked to two gallium atoms. The bonds that link two of the three sulfur atoms to three gallium atoms consist of two covalent bonds and a third dative bond, while the third sulfur atom linked to two gallium atoms represents the bridging atom. The addition of La_2S_3 brings in an additional S^{2-} anion that results in modification of the dative bond of the trigonally coordinated sulfur atom. The dative bond is broken and the S^{2-} anion provided by the modifying rare-earth sulfide helps in restoring and maintaining the tetrahedral environment of GaS_4, at the same time creating a negative site for the La^{3+} cation. Lucazeau et al. [19] studied the structure of these glasses using Raman spectroscopy. The Raman spectra of the glasses and of similar crystalline phases were compared and spectral differences were found between the two glassy and crystalline states. This has been interpreted in

terms of structural modification of the short-range periodicity around the Ga atoms, although there was no conclusive evidence.

1.3 Electronic Properties of Chalcogenide Glasses

Chalcogenide glasses can be characterized as being variously covalent, metallic, and ionic. In covalent chalcogenide glasses such as Se and As_2S_3, the so-called 8-N rule applies to the coordination number of the constituent atoms, e.g. the coordination number of chalcogens is generally 2 since the total number of valence electrons is $N = 6$. The magnitude of the band gap is 1–3 eV depending on the composition, the band gap increasing in the series Te → Se → S. Electrical conduction in many chalcogenide glasses is governed by holes. Accordingly, these glasses can be regarded as amorphous semiconductors. However, in a glass containing large amounts of Te, the band gap decreases (∼1 eV), and the metallic character increases. Moreover, in glasses such as Ag–As(Ge)–S, the coordination number of S is demonstrated to be 3–4 [20], and ionic conduction of Ag^+ governs the electrical conductivity. So these glasses can be considered as ionic glasses or ion-conducting amorphous semiconductors.

1.3.1 Electronic States in Chalcogenide Glasses

If we compare the optical properties of crystalline and amorphous As_2S_3 and As_2Se_3, we see that the effect of disorder on the electronic structure is relatively small; the optical absorption edges (band gaps) are very similar. The major difference between crystalline and amorphous solids lies in a higher density of traps and a larger energy distribution of the trapping levels in the amorphous solid. The electrical band gap for As_2Se_3 is 1.1 eV in comparison to 1.9 eV for the optical gap. The optical gap is therefore approximately double the electrical gap, which indicates that the Fermi level is situated near the middle of the mobility gap (the energy interval between the demarcation levels between localized and extended states in valence and conduction bands). In a chalcogen, e.g. selenium, the four 4p electrons occupy two bonding orbitals representing covalent bonding and one orbital named a lone-pair orbital, which does not participate in the covalent bonding. The p electrons give rise to strong covalent bonds. Lone-pair electrons determine the dihedral angles and, being the uppermost electrons in the valence band, play an important role in defining the energy bands.

Various experimental techniques have been used to determine the density of localized states in the gap. It was concluded from transient photocurrent-decay measurements that the density of tail states decreases exponentially and does not have any defined structure [21]. It is now generally believed that, on top of a featureless distribution of states in the tails, a structured density of states exists, attributed to valence alternation pairs (VAPs)) [22]. For arsenic

triselenide, time-of-flight and transient photoconductivity measurements suggest a feature located 0.6 eV above the valence band edge which dominates the transport. There has been some controversy in the literature related to the sign of the correlation energy in amorphous selenium. While Kastner et al. [23] originally assumed a negative correlation energy, early theoretical work [24] indicated that, in fact, the correlation energy in a-Se should be positive, i.e. spin pairing at coordination defects would be energetically unfavorable. Recently, it was demonstrated by Kolobov et al. [25], using light-induced ESR, that the correlation energy was indeed negative. Popescu [26] has stated that in amorphous selenium the defect states C_3^+ (where C stands for chalcogen and the superscript and subscript gives the charge and coordination, respectively) give rise to discrete traps situated at around 0.33 eV below the bottom of the conduction band and they control the electron mobility. The C_1^- defect states are situated at 0.17 eV above the top of the valence band and control the hole concentration. Both types of traps are distorted by trapping of the charge carriers, and, as a consequence, their energies do not correspond to that found from light-absorption experiments and charge-carrier generation.

Tanaka has recently proposed [27,28] a model of a realistic density of states based on several experimental results (Fig. 1.3a). Spatial potential fluctuations and the atomic structure in As_2S_3 are shown schematically in Fig. 1.3b, c, respectively. In this model, it is assumed that the Urbach edge arises from fluctuations of the van der Waal's type interlayer bonds and/or disordered interactions among the intralayer lone-pair electrons. The weak absorption tail in this model is ascribed to transitions involving antibonding states of As–As wrong bonds, which can produce unoccupied deep states below the conduction band. Electronic excitations can generate localized holes in the valence-band edge and delocalized electrons in the conduction band. The other possibility is generation of delocalized holes in the valence band and localized electrons in the conduction-band tail. Excited carriers are immediately ($\approx 10^{-12}$ s) trapped into the localized states.

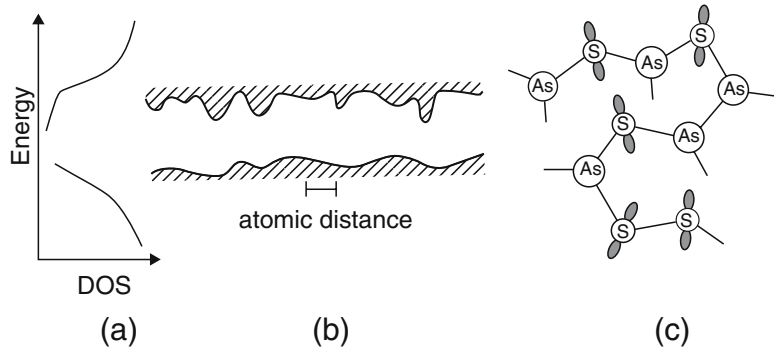

Fig. 1.3. (**a**) Density of states, (**b**) the spatial potential fluctuations and (**c**) the corresponding atomic structure proposed for As_2S_3 glass (after [20])

1.3.2 Measurements of the Absorption Coefficient and the Optical Gap

The optical absorption edge in amorphous semiconductors is generally not as steep as that in crystalline semiconductors. In general, the absorption spectrum $\alpha(\hbar\omega)$ can be divided into three parts [29] (see Fig. 1.4). For $\alpha \geq 10^4 \mathrm{cm}^{-1}$, the spectrum shows a square-root dependence, $\alpha\hbar\omega \propto (\hbar\omega - E_\mathrm{g}^\mathrm{T})^{1/2}$.

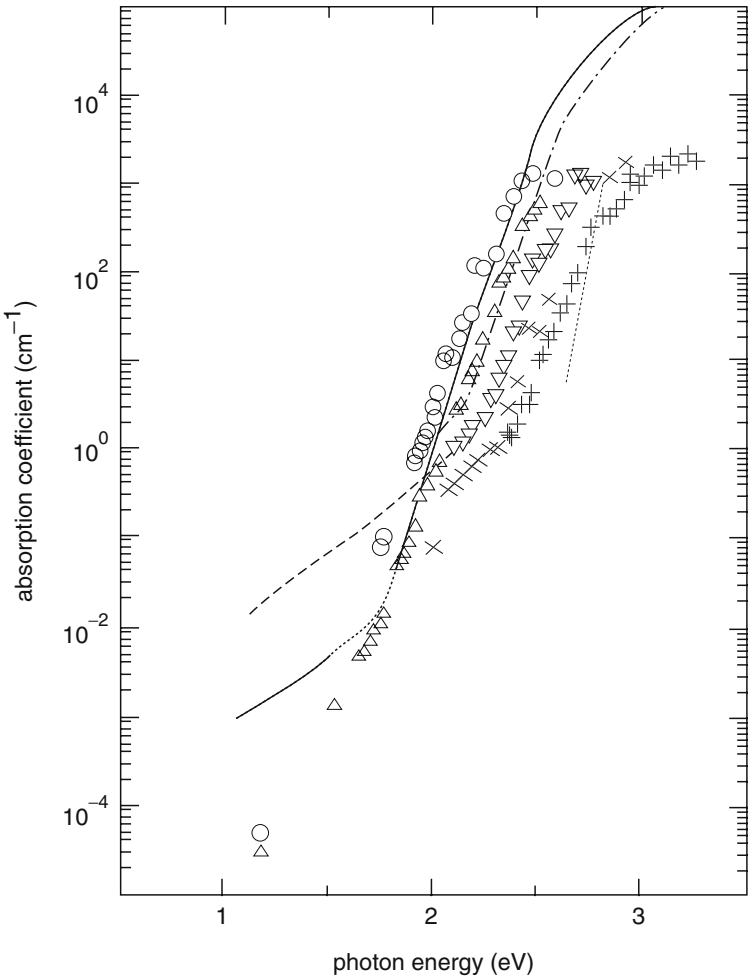

Fig. 1.4. Optical absorption edges in As_2S_3 glasses at different temperatures. The two lines (*solid* and *dashed*) show absorption spectra for different samples at 300 K. Spectra at 175 K(*plus*), 200 K (*times*), 250 K (*downtriangle*), 300 K (*triangle*), and 400 K (*circle*) have been obtained under 10^5 V cm^{-1} using the constant-photocurrent method. Also shown are spectra at 10 K for As_2S_3 glass (*dot-dashed line*) and for a crystalline sample (*dotted line*) (after [30])

For $10^4 \geq \alpha \geq 10^0\,\mathrm{cm}^{-1}$, the so-called Urbach edge with the form of $\alpha \propto \exp(\hbar\omega/E_\mathrm{U})$ appears. For $\alpha \leq 10^0\,\mathrm{cm}^{-1}$, a weak-absorption tail with $\alpha \propto \exp(\hbar\omega/E_\mathrm{W})$ exists. In the above, E_g^T represents the optical (Tauc) gap. In As_2S_3 glass at room temperature, for example, $E_\mathrm{g}^\mathrm{T} = 2.36\,\mathrm{eV}$, $E_\mathrm{U} \approx 50\,\mathrm{meV}$, and $E_\mathrm{W} \approx 250\,\mathrm{meV}$ [29–31]. It should be noted that the mobility gap, which can be evaluated from photoconduction spectra, appears to be located at ≈2.5 eV [30, 32].

The absorption coefficient, α, of chalcogenide films has been measured using several techniques for as-deposited, annealed, and photodarkened films, as well as in fabricated waveguides. At short wavelengths, where the absorption is high, a conventional spectrophotometer could be used, with corrections for reflection losses using the method described in [33]. At wavelengths beyond the band edge, however, the absorption is too small for this technique to be useful. Photothermal deflection spectroscopy (PDS) has therefore been used [31] to measure the relative absorption coefficient in the long-wavelength region. To calibrate the PDS data, absorption values from the spectrophotometer and the PDS are overlapped in the region of moderate absorption just beyond the band edge, where both give an accurate measurement. In addition, optical loss can be determined at spot wavelengths from propagation measurements made in slab waveguides.

For these measurements [34], films deposited onto oxidized Si wafers were placed in a prism coupler, and the lowest-order slab waveguide mode was excited. Some radiation was scattered from the surface of the sample and could be detected using a cooled CCD camera. At wavelengths close to the absorption edge (633 nm), the decay of the intensity with distance was assumed to be dominated by film absorption, and hence the absorption coefficient for the film could be determined and used to calibrate the PDS data. The results of PDS measurements showed that as-deposited As_2S_3 films have losses below $0.1\,\mathrm{dB\,cm}^{-1}$ across the telecommunications band at 1,300 and 1,550 nm [34]. Films that were 2.5 μm thick were used for single-mode waveguide fabrication using a direct-writing system. To assess the losses in fabricated waveguides, it was found possible to image the light scattered from the waveguides and to monitor the decay of the power in the waveguide as a function of distance using an IR-sensitive video camera. Light from laser-diode sources at 780, 1,300, and 1,550 nm was end-coupled into the waveguides using a microscope lens for these measurements. The losses obtained in this way were $\sim 0.4\,\mathrm{dB\,cm}^{-1}$ at 780 nm, $\sim 0.24\,\mathrm{dB\,cm}^{-1}$ at 1,300 nm, and $0.2\,\mathrm{dB\,cm}^{-1}$ at 1,550 nm [34]. These values are in good agreement with those obtained from the PDS measurements. The output from the waveguides was imaged with a microscope objective onto a video camera. The waveguides were single mode at 1,300 nm and 1,550 nm.

Band theory for crystalline semiconductors suggests that the absorption coefficient for indirect transitions can be written as

$$\alpha = \mathrm{const} \times M^2 \frac{(h\nu - E_\mathrm{g})^2}{h\nu} \tag{1.1}$$

Table 1.1. Optical gap for evaporated films (after [35])

composition	$E_g(eV)$
As_2S_3	2.26
As_3Se_{97}	1.935
$As_{22}Se_{78}$	1.872
$As_{41}Se_{59}$	1.79
$As_{39}Se_{61}$	1.79
$Ge_9As_{25}Se_{66}$	1.922
$Ge_5As_{35}Se_{60}$	1.828
$Ge_2As_{40}Se_{58}$	1.783

The optical gap for As_2S_3 is for PLD deposited films [34]

Table 1.2. Optical gap for some bulk chalcogenide glasses (after [36])

glass	$E_g(eV)$
$Ge_{25}Se_{75}$	2.07
$Ge_{25}Se_{65}Te_{10}$	1.73
$Ge_{28}Se_{60}Sb_{12}$	1.8
As_2Se_3	1.77
As_2S_3	2.4

The optical gap for As_2S_3 is taken from [37]

where M is the matrix element of the optical transition and E_g is the band gap energy.

The absorption in many amorphous semiconductors is observed to obey this relation above the exponential Urbach edge. If M is constant, plotting $(\alpha h\nu)^{1/2}$ versus $h\nu$ should result in a straight line. The optical gap, E_g, is obtained from the intersection of this line with the energy axis. The value obtained for the optical gap of pulse laser deposited (PLD) a-As_2S_3 film was $E_g = 2.26 \pm 0.02$ eV [34]. This value is slightly lower than that of 2.36 eV found for thermally evaporated As_2S_3 films, most probably due to illumination of the films during the laser-deposition process. Table 1.1 shows the results of optical-gap measurements for evaporated chalcogenide films, while the optical gaps of some chalcogenide glasses are shown in Table 1.2.

1.4 Chalcogenide Glasses for Near-Infrared Optics

A range of optical functions can be realized in these glasses, including optical amplification and emission at telecommunication wavelengths by rare-earth (e.g., Pr and Er) dopants, fabrication of waveguides (channel, self-written, femtosecond written), that can laterally or vertically couple light to various locations within a planar structure, and gratings (relief and phase) that can spectrally filter or modulate light. Diffraction gratings have been fabricated

in chalcogenide glasses using the photoinduced effects that they exhibit. Both photodarkening [38] and the metal-photodissolution effect [40] (especially of silver) have been used to fabricate transmissive gratings, especially for use at IR wavelengths. A variety of techniques have been used to fabricate these gratings, including holographic, mask exposure, or etching methods. These gratings can be used as efficient beam combiners, couplers and have significant applications in monochromators, laser-tuning devices, shapers, optical-fiber couplers, etc. For instance, gratings have been written holographically in sputtered $Ge_{10}As_{40}S_{25}Se_{25}$ films with 514.5 nm light from an Ar-ion laser and probed with a 670 nm diode laser [38]. The probe was highly attenuated to avoid influencing the photodarkening process. The first-order efficiency of Raman–Nath diffraction for a probe beam tuned to the Bragg condition was used to measure a refractive-index change of $\Delta n = 0.001$ for a written intensity of $100\,\mathrm{mW\,cm^2}$. Slinger et al. [39] recorded volume holographic gratings in evaporated $As_{40}S_{60}$ films in which silver was photodissolved. They measured the angular response of the gratings, and replay was made in air using light of wavelength 632.8 nm from a helium–neon laser. Typical Bragg behavior was observed and the diffraction efficiency in the first-order diffracted beams reached a maximum of 9% near the Bragg angle. A photolithographic technique has been used [40] to fabricate surface-relief gratings in a bi-layer structure consisting of a 0.8 µm a-$As_{30}S_{70}$ film and an under-layer of Ag of 0.14 µm thickness. Thin gratings produced by mask exposure showed Raman–Nath type diffractive behavior and, when replayed at 632.8 nm, first-order diffraction efficiencies of up to 10% were measured. First- and second-order Bragg reflectors at telecommunication wavelengths (1.5 µm) have been fabricated in single-mode monolayer (As_2S_3) and multilayer (As–S–Se/As–S) chalcogenide glass planar waveguides with near-band gap illumination using an interferometric technique [41]. Reflectivities as high as 90% near 1.55 µm, and refractive-index modulations up to 3×10^{-4} were achieved. The volume photodarkening effect is the principal mechanism involved in the formation of the Bragg gratings. The stability and high efficiency of these gratings make them potentially useful as wavelength-selection elements, and add-drop filters for WDM networks [41].

Richardson et al. [42] have written permanent waveguides in both bulk and film of As_2S_3 glasses [43]. Using a train of 850 nm femtosecond laser pulses, they measured both the induced index variation and structural changes induced through the photomodification. The refractive-index variation between the waveguide (exposed region of the glass sample) and the cladding (unexposed region) was evaluated following waveguide writing. An induced index change of $\Delta n = -0.04$ was associated with the formation of a 9 mm diameter circular waveguide formed by moving the sample through a well-characterized focal region [41]. A key finding of the study defined the structural mechanism associated with the writing process in the As_2S_3 material. The concurrent destruction of As–S bonds within the glass network and the associated formation of As–As bonds during the bulk material

modification was quantified by a two-dimensional micro-Raman analysis (excitation with $\lambda \approx 752\,nm$).

Optical amplification at 1.083 µm in neodymium-doped chalcogenide fibers was observed [44] in a glass composition of Ge–As–Ga–Sb–S. A maximum internal gain of 6.8 dB was achieved for a pump power of 180 mW. The first amplified spontaneous emission in a chalcogenide glass fiber has also been reported [44]. Laser action in a rare-earth-doped GaLaS chalcogenide glass has been demonstrated, showing that this class of glasses is suitable for active applications, such as amplifiers and lasers [45]. A neodymium-doped GaLaS glass laser has been operated under continuous-wave conditions at a wavelength of 1.08 µm when pumped with a Ti:Sapphire laser at either 0.815 or 0.890 µm [45]. The reasonably low laser threshold indicated acceptable glass losses, but the laser performance was worse in comparison with conventional Nd-lasers. The original application of GaLaS glass was as a practical and efficient 1.3 µm optical fiber amplifier.

The ability to move and manipulate light without using costly and delicate articulated arms and mirrors is a common requirement for several applications, e.g., laser surgery. Power handling of GaLaS fibers has been assessed by coupling to an Nd:YAG laser operating at 1,064 nm. A total of 5 W of power was guided through a core of about 150 µm with no apparent laser damage [46].

1.5 Chalcogenide Glasses for Mid-IR and Far-IR Applications

A selenide glass has been developed that can be doped with rare-earth ions and is stable against crystallization during fiberization [47]. The glass is based on GeAsGaSe and can be doped with Pr^{3+} and Dy^{3+} for near- and mid-IR applications. The doped glasses have been fiberized with core-only losses of $0.8\,dB\,m^{-1}$ at 6 µm and $1.5\,dB\,m^{-1}$ at 2.5 µm. Single-mode fibers have been drawn with a measured core loss of $3\,dB\,m^{-1}$ at 1.55 µm.

Pr^{3+} incorporation has been investigated and mid-IR emission in the 3–5 µm region has been observed. Schweizer et al. [48] have found that the absorption spectrum of a 9.7 mol% Er^{3+}-doped GaLaS glass showed excellent rare-earth solubility and the potential for high doping concentrations and hence short devices; this represents a major advantage of GaLaS glass compared with conventional chalcogenide glasses, which suffer from very low rare-earth solubilities. Values obtained for branching ratios of 1% for both the 3.6 and 4.5 µm transitions, with measured lifetimes of 100 and 590 µs and cross-sections of 0.43×10^{-20} and $0.25 \times 10^{-20}\,cm^2$, were in good agreement with the results of [49], respectively, in an Er^{3+}-doped barium indium gallium germanium sulfide glass. The radiative properties of Er^{3+}-doped Ga–La–S lend themselves to applications. Radiation at 2 µm has application in LIDAR systems, radiation at 2.75 µm coincides with a strong water absorption

in tissue and is used for medical applications, the 3.6 µm transition could be useful for H_2S, NO, and SO_2 (remote) sensing and the 4.5 µm transition could find use in CO and O_3 gas sensors when tuned to 4.7 µm. High-power CO and CO_2 lasers operating at 5.4 and 10.6 µm, respectively, are available and are used for industrial welding and cutting. Transmitting the laser power through fibers enables remote operation to take place. Te-based fibers have demonstrated output powers of 10.7 W for 19.4 W launched power (efficiency = 55.2%) at 10.6 µm [50]. The fibers possessed an antireflection (AR) coating and were cooled with water to prevent thermal lensing caused by an increase in absorption coefficient with temperature ($d\alpha/dT$) and an increase in refractive index with temperature (dn/dT). On the other hand, arsenic sulfide-based fibers have demonstrated 85 W output power for 169 W launched power (efficiency = 50.3%) without the need for cooling and AR coatings [51]. Unlike the Te-based glasses, arsenic sulfide-based glasses have smaller values of $d\alpha/dT$ and dn/dT . Typically, the fiber diameters are usually in excess of 500 µm for high-power laser delivery to reduce the power density. However, small core diameter (<200 µm) fibers have demonstrated a tolerance to power densities of 125 kW cm^{-2} at 5.4 µm and 54 kW cm^{-2} at 10.6 µm without damage [52]. The arsenic sulfide fibers transmit in the 2–5 µm region and can be used for transmission of laser power in this region for military applications, such as in infrared countermeasures and laser threat-warning systems [53]. The output power versus input power for a sulfide fiber using a pulsed laser operating in the 2–5 µm region has been measured [54]. The average power was about 2.69 W, but the peak power was 26.9 kW which corresponds to the largest input power density, 1.07 GW cm^{-2}, without fiber damage for $\leq 1.5 \times 10^7$ pulses [54]. This threshold of about 3.0 GW cm^2 is due to dielectric breakdown at the surface. Recent efforts have considered delivery of energy from a medical free-electron laser (MFEL) operating between 2 and 10 µm through chalcogenide fibers [55]. The MFEL can emit more than 10 MW of power in a femtosecond pulse, which relates to an average power of greater than 10 W. It has been shown [2, 56] that surgery at 6.45 µm based on cleaving of protein bonds is more efficient and leads to less denatured tissue and scarring than with conventional Er:YAG lasers operating at 2.94 µm based on OH absorption [2, 56].

Chalcogenide fibers are well-suited for chemical-sensing applications, since most molecular species vibrate in the infrared region. Chalcogenide fibers can be used in fiber-optic chemical-sensor systems for quantitative remote detection and identification, as well as detecting chemicals in mixtures. Different sensing techniques including attenuated total reflectance (ATR) [57–59], diffuse reflectance, and absorption spectroscopy [60–62] have been introduced. Numerous systems have been studied which include oil, freon, soap, paints, polymer-curing reactions, glucose/water, benzene and derivatives, chlorinated hydrocarbons, alcohols, carboxylic acids, aqueous acids, perfumes, and pharmaceutical products.

For example, a fiber-optic dipstick probe could monitor the quality of engine oil and, consequently, save large amounts of money in preventing unnecessary oil changes in the military and civil sector. A fiber optic-based reflectance probe has been used to detect contaminants in soil [63]. Detection limits of 130 ppm of marine diesel fuel in sea sand have been demonstrated using a 20-meter length of cable. A chalcogenide-fiber ATR probe has been used to show the spectral differences between various tissues and organs in biomedical samples. IR spectra in the region of 2–10 μm for various organs/tissues from a dead chicken, as well as from the liver of an anaesthetized sheep [55], have been recorded. Chalcogenide fibers can be utilized to generate a biomedical database for medical diagnostics, such as tissue evaluation and early detection of cancer [64].

Ueda et al. [65] have used As–S fibers with a Teflon cladding to measure temperature increases of up to 200°C on the surface layer of ceramic plates during grinding. Chalcogenide fibers have also been used for thermal imaging [66]. Saito et al. [67] recorded the image of an electric iron at 773 K through a 1,000 fiber bundle, and Nishi et al. [68] fabricated a flexible fiber bundle containing 8400 Teflon-coated fibers and recorded the thermal image of an operating integrated circuit in the 3–5.4 μm region. Hyperspectral imaging can be exploited by coupling coherent fiber bundles to focal-plane array (FPA) detectors based on InSb (2–5.4 μm) detectors. Focal-plane array detectors are extremely sensitive and can be used for performing both spatial and spectral analyses in the infrared [69].

A 10×10 bundle of As_2S_3 fibers with a Teflon cladding was reformatted to a 1×100 array and the output analysed using a grating spectrometer [70]. High-quality single-mode and multimode chalcogenide fibers have been used to demonstrate 100 nm resolution for both topographic and spectroscopic analyses of polycrystalline diamond [71]. The material that is most widely used in fiber optics is currently silica, which provides a transmission window that extends to only about 2 microns. With their high glass-transition temperature, GaLaS glasses offer the potential for greater power handling capacity. Lasers with emission wavelengths around 2.9 microns are widely used in surgery. This wavelength corresponds to the strongest absorption band of water and thus bio-tissues, allowing a host of medical applications [72].

1.6 Bulk Chalcogenide Glasses, Composition, and Optical Constants

In order to synthesize chalcogenide glasses, the appropriate chemical elements (e.g., 99.999% pure), in the quantities required for producing the desired composition, are placed in a pre-cleaned quartz ampoule. After evacuating the residual gases to a pressure of 10^{-5} Torr, the ampoule is sealed under vacuum and placed in a furnace, where melting of the components takes place at

temperatures between 600°C and 970°C (depending on composition). In order to achieve good homogenization of the chalcogenide glasses and to produce glasses with uniform composition, the furnace can be slowly rocked during the time the ampoule is at high temperature. The ampoule is cooled down to 350–400°C at a rate of $\sim$100°C h^{-1}. At this temperature, the ampoule containing the synthesized material is left in air or is cooled rapidly in cold water. Whereas most chalcogenides are melted in sealed ampoules containing the required amounts of elemental precursors, gallium lanthanum sulfides are melted from prepared batches of Ga_2S_3, La_2S_3, and La_2O_3. Batches of powders are placed in a vitreous carbon crucible and melted in a tube furnace at 1,150°C for typically 24 h, depending on the batch size. The molten Ga_2S_3 fluxes the lanthanum precursors, incorporating them into the liquid at temperatures much lower than their melting point. After quenching the resulting melt, the glasses are then annealed near the glass-transition temperature. The composition of bulk glasses can be determined in a scanning electron microscope with an X-ray microanalyzer [73]. The mean data for the element content in a selection of the bulk glasses, including some of those exhibiting the greatest changes in optical properties, has been presented [74]. It was shown that the compositions of bulk glasses were generally within $\sim$1 at.% of the expected compositions. Some crystalline phases were observed in $As_{45}S_{55}$ and also in the Ge–S–Tl bulk glasses (C–As_4S_4 and α-GeS_2, respectively). The binary gallium lanthanum sulfide system has a maximum stability for a gallium-to-lanthanum ratio of 70:30 [75]. Glass formation extends from about 60:40 to 80:20 for this two-component glass. Through the addition of a third or fourth component to the basic GLS glass, a wide range of modified compositions with varying properties can be realized. A wide range of modifiers have been tested. This was originally motivated by the quest for glass stabilizers, additional components that would improve the thermal characteristics of the glass and thus aid fiber drawing. The majority of attention has focused on the addition of oxides, in particular, lanthanum oxide in GLS glass. It is now believed that a small percentage, typically 1–2 weight percent of lanthanum oxide, is essential for glass stability. The addition of oxide radically improves the thermal stability of the glass but at the expense of its phonon energy and thus of the potential for active optical applications.

Different techniques have been used to measure the optical constants of chalcogenide glasses. For bulk samples, normally an optical transmission curve of the sample at different thicknesses, together with reflection data, is needed to calculate both the dispersion and the absorption characteristics of the sample [76,77]. Table 1.3 summarizes, for some of the glass systems examined [78], the optical band gap energy and the refractive index as measured in the mid-infrared.

Tables 1.4–1.7 show the results of refractive-index measurements for some other chalcogenide systems examined at different wavelengths using various methods.

Table 1.3. Optical band gap and refractive index measured at 10.6 μm for several chalcogenide glass compositions (after [78])

nominal composition (mol%)	$E_g(eV)$	n
$As_{40}S_{40}Se_{20}$	1.70	2.47
$As_{24}S_{38}Se_{38}$	1.67	2.32
$As_{37}S_{56}Se_7$	1.79	2.43
$Ge_{30}As_{11}Se_{49}Te_{10}$	1.22	2.50
$Ge_{17}As_{18}S_{26}Se_{39}$	1.64	2.41
$As_{30}Se_{63}Sb_4Sn_3$	1.28	2.80
$Ge_{28}Sb_{12}Se_{60}$	1.39	2.60
$Ge_{25}Ga_5S_{70}$	2.38	~ 2
$Ga_{28}La_{12}S_{60}$	2.38	2.50
$Ga_{24}La_{10}S_{60}Ce_6$	2.17	2.54

Table 1.4. Optical properties of GeS_2-based glasses measured using ellipsometry (after [79])

composition (mol%)	n at 633 nm
$x = 0$	2.01
$x = 10$	2.15
$x = 20$	2.21
$x = 30$	2.25
5-a: $(100 - x)GeS_2 - xGa_2S_3$ glasses	
composition (mol%)	n at 633 nm
$x = 0$	2.25
$x = 10$	2.20
$x = 15$	2.17
$x = 20$	2.14
5-b: $70GeS_2 - (30 - x)Ga_2S_3 - x$CdS glasses	
composition (mol%)	n at 633 nm
$x = 0$	2.01
$x = 10$	2.12
$x = 20$	2.15
$x = 30$	2.17
$x = 40$	2.19
5-c: $(100 - x)GeS_2 - x[0.5Ga_2S_3 - 0.5$CdS] glasses	

Table 1.5. Optical properties of $Ge_{10}As_{10}Se_{80-x}Te_x$ glasses: n_s, values measured using the cut-back method; n_E, values measured using ellipsometry (after [80])

glasses	n_s at 1,550 nm	n_E at 1,550 nm	n_s at 1,050 nm	n_E at 1,050 nm
x = 0	2.58	2.52	2.66	2.56
x = 10	2.74	2.60	2.82	2.63
$x = 15$	2.80	2.69	2.90	2.75
$x = 20$	2.90	2.73	2.95	2.81

Table 1.6. Optical properties of some chalcogenide glasses (after [81])

glass	n at 1.55 µm	λ_{gap} (µm)
$As_{40}S_{60}$	2.45	0.52
$As_{40}S_{50}Se_{10}$	2.49	0.55
$As_{40}S_{40}Se_{20}$	2.55	0.59
$As_{40}S_{30}Se_{30}$	2.62	0.62
$As_{40}S_{20}Se_{40}$	2.70	0.64
$As_{40}S_{10}Se_{50}$	2.76	0.67
$As_{40}Se_{60}$	2.81	0.70
$As_{39}Se_{61}$	2.81	0.70
$As_{40}Se_{55}Cu_5$	2.93	0.79
$As_{25}S_{55}Te_{20}$	2.52	0.79

Table 1.7. Optical properties of GeS_2-based glasses (after [82])

Glass	n at 633 nm
$(GeS_2)_{85}(Ga_2S_3)_{15}$	1.9940
$(GeS_2)_{85}(Ga_2S_3)_{11}(CsI)_4$	2.1600
$(GeS_2)_{75}(Ga_2S_3)_{10}(CsI)_{10}(Ag_2S)_5$	2.1445

1.7 Chalcogenide Thin Films and Comparison with the Bulk

As the properties of a glass are a function of its thermal history, it is not unexpected that films or fibers may have properties that vary from those seen in their melt-derived bulk analogues. Films can be deposited, by thermal evaporation of their parent bulk glasses, onto room-temperature, pre-cleaned substrates under a vacuum of nominally between 10^{-5}–10^{-7} Torr. Glassy films prepared by this technique have been confirmed to be amorphous in nature and can vary in composition from the parent bulk by less than 5 at.% [79]. The refractive index can be obtained using transmission-curve or prism-coupling techniques [83] or a grating-coupling technique [84].

The absorption coefficient and the band gap can be calculated using transmission data. PDS has been used [31] to measure low values of the optical absorption coefficient of chalcogenide glasses in the form of thick samples, as well as films. PDS has been applied to optical-absorption measurements in, for example, As_2S_3 and As–S glasses [31]. This spectroscopic method has been demonstrated to be suitable for the evaluation of low absorption in thin samples, although its accuracy is affected by light scattering. For As_2S_3, as-evaporated films have a higher residual absorption than that of the bulk. As compared with changes in bulk-glass refractive indices, in the As–S–Se system, the film indices exhibited slightly larger variations with composition. This variation may be attributable to subtle compositional variations and the higher cooling rate with which the film structure assembles from the vapor

phase. The ability for molecular species to occur in the vapor phase [11] would give rise to a notably more ordered, connected molecular structure as compared with systems where little or no molecular ordering is believed to occur (e.g., in ternary As–S–Se glasses). Annealing of as-deposited films results in a further increase in refractive index and density, as the frozen network structure relaxes and further polymerizes.

Up to now, thermal evaporation and sputtering have been used to produce chalcogenide amorphous thin films. A significant problem encountered with these films is associated with the need to anneal them before light exposure for waveguide writing. In general, their thermal-expansion coefficient is much larger than common substrate materials, such as fused silica or silicon, leading to cracking or film lift off during or after annealing. While rapid thermal annealing [38] has proven a useful approach to minimize these problems, any deposition process that removes the need for annealing would have a significant advantage. Pulsed-laser deposition (PLD) is another technique for depositing chalcogenide films. A well-known advantage of the PLD technique is that it can accurately transfer the stoichiometry of a multicomponent target to a film deposited on a substrate. This is particularly important in materials containing weakly bonded volatile components such as sulfur, where thermal evaporation often results in marked changes in stoichiometry. In addition, PLD can result in bombardment of the substrate by relatively high-energy ions or neutral species, and this assists in densification of the film in a way analogous to the use of ion bombardment during sputtering. It is possible, therefore, for PLD to produce high-quality films that do not require annealing, as is generally essential for thermally evaporated films. A disadvantage of the conventional PLD process, which uses high-energy ($\sim$1 J), low-repetition rate (10–100 Hz) nanosecond laser pulses, is the production of particulates that can lead to high scattering losses in the films. It has been previously shown that the problem of particulates produced by conventional PLD can be eliminated by using an ultrafast PLD process that employs short ($<$50 ps), low-energy ($\sim\mu$J), high-repetition-rate (10^5–10^8 Hz) pulse trains [85, 86]; indeed, it was possible to produce high optical quality As_2S_3 chalcogenide glass films using ultrafast PLD [87]. The surface quality of the deposited films was almost down to the atomic level, with an rms roughness of the order of 0.42 nm. The resulting films were highly photosensitive and could be used without thermal annealing for waveguide fabrication using the photodarkening process. The prism-coupling technique [34] was used to measure the refractive index at 632.8, 810, and 1,064 nm for films deposited onto fused-silica microscope slides or onto silicon wafers covered by an oxidized layer 2.4 μm thick. During these measurements, the ability of the films to act as waveguides could also be assessed from propagation of the excited slab waveguide modes. In general, rather poor propagation was observed at 633 nm due to strong absorption (10–20 dB cm^{-1}) of the films due to the proximity of the band edge, whilst at longer wavelengths the losses were relatively low (a few dB cm^{-1} or lower). The beams propagating in

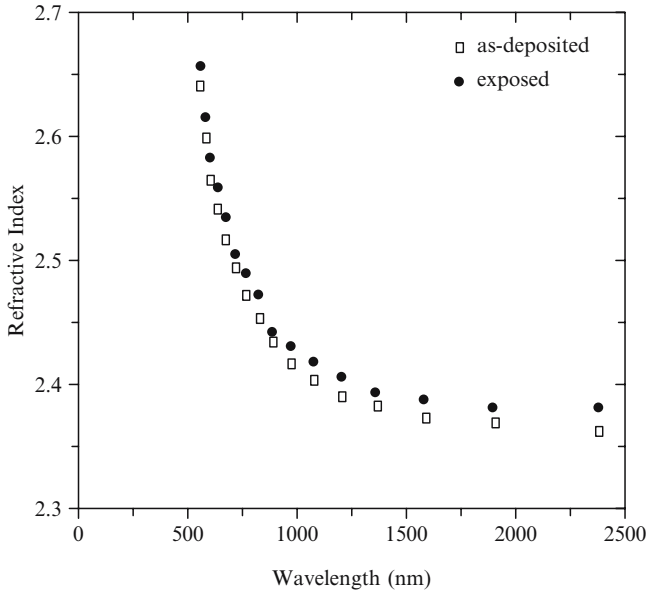

Fig. 1.5. Refractive index of MLQS As_2S_3 films versus wavelength. Samples were exposed by a green laser beam and the illumination intensity was 10 mW mm^{-2} (after [88])

the planar slabs could be discerned from scattering of the propagating light, indicating that scattering centers had not been totally eliminated. In order to characterize more broadly the refractive indices of the films, a transmissivity measurement was performed using a spectrophotometer. The dispersion characteristics of the material were extracted from interference fringes present on the transmission curve, via the Swanepoel technique [77]. Figure 1.5 shows a typical spectral dependence of the refractive index for one of the mode-locked Q-switched (MLQS) films. The results were reproducible to 0.01 over different deposition runs. Similar results were obtained for the films deposited using a purely mode-locked (PML) laser ($\lambda = 532\,nm$), although the as-deposited refractive index was generally about 0.01 lower than (MLQS) deposited films.

In order to examine the effect of laser exposure on these films, an area of a few cm^2 of the sample was scanned with a 514.5 nm, cw laser beam (the illumination intensity was 10 mW mm^{-2}) with a total fluence of 1,000 mJ mm^{-2}. Refractive indices of the illuminated area were again measured using the above techniques. Figure 1.5 shows also the spectral dependence of the refractive index of the illuminated area. In this case, a significant difference in the exposure characteristics was observed for the MLQS films compared with the PML films. In the former case, a photoinduced change of $\Delta n_{\mathrm{MLQS}} \approx +0.01$ in refractive index was measured over the whole wavelength range,

whilst in the latter, the index change was much bigger $\Delta n_{\mathrm{PML}} \approx +0.04$. In both cases, the index change could, in principle, be exploited for waveguide fabrication. In order to prepare a film with the lowest number of scattering centers, extensive work on the effects of annealing of these films was carried out [88]. Normally, annealing removes all stress and strain in films and hence produces a more relaxed glass structure for device fabrication. Figure 1.6 shows the index change as a result of annealing of MLQS films in a nitrogen environment. As can be seen, a change of refractive index up to 0.04 was observed as a result of annealing of films at 150°C. No detectable change in composition was observed for the films when annealed up to 150°C.

Tables 1.8 and 1.9 summarize the result of optical-constant measurements for chalcogenide films prepared by different deposition techniques and under different heat-treatment procedures, while Figs. 1.7 and 1.8 show results of optical-constant measurements versus wavelength for $Ge_xSb_yTe_z$ films [89].

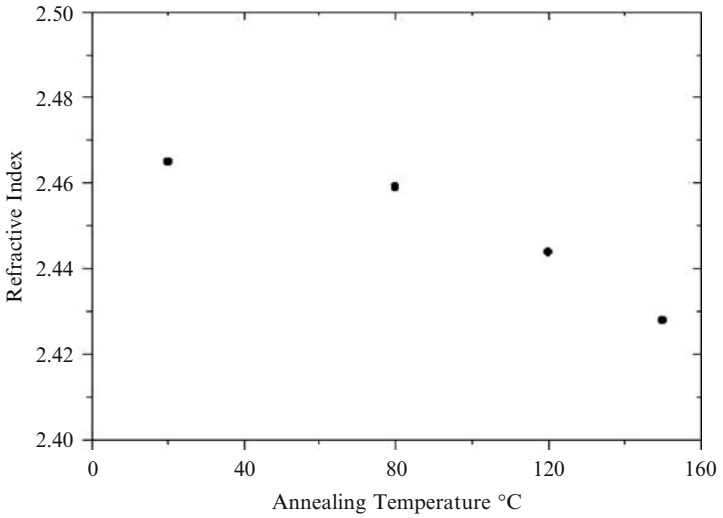

Fig. 1.6. Effect of annealing on the refractive index of an As_2S_3 film measured at 810 nm (after [88])

Table 1.8. Optical constants of thin $Ge_xSb_yTe_z$ films (after [89])

material	deposition method	n at 635 nm	k at 635 nm	n at 650 nm	k at 650 nm	n at 780 nm	k at 780 nm	n at 830 nm	k at 830 nm
$Ge_8Sb_{23}Te_{59}$	evap.	4.38	2.27	4.43	2.22	4.83	1.77	4.92	1.58
$Ge_{14}Sb_{28}Te_{58}$	sputt.	4.39	2.08	4.46	2.04	4.77	1.65	4.80	1.47
$Ge_{22}Sb_{22}Te_{56}$	sputt.	4.31	1.90	4.36	1.85	4.62	1.46	4.72	1.3

Table 1.9. Optical constants of evaporated chalcogenide films (after [10])

composition	n at 1.53 µm	n at 1.55 µm	film status
$As_{40}S_{60}$	2.4035	2.4050	annealed
$As_{40}S_{60}$	2.3439	2.3439	not annealed
$As_{36}S_{59}Se_{15}$	2.4707	2.4636	annealed
$As_{40}S_{45}Se_{15}$	2.4139	2.4098	not annealed
$As_{39}S_{29}Se_{32}$	2.5727	2.5709	annealed
$As_{40}S_{30}Se_{30}$	2.5074	2.4949	not annealed
$As_{40}S_{14}Se_{46}$	2.6750	2.6766	annealed
$As_{40}S_{15}Se_{45}$	2.6239	2.6270	not annealed
$As_{40}Se_{60}$	2.8318	2.8318	annealed
$As_{40}Se_{60}$	2.7842	2.7707	not annealed
$As_{32}S_{34}Se_{34}$	2.5400	2.5414	annealed
$As_{32}S_{34}Se_{34}$	2.5050	2.5041	not annealed
$As_{24}S_{38}Se_{38}$	2.4666	2.4650	annealed
$As_{24}S_{38}Se_{38}$	2.4445	2.4445	not annealed
$As_{18}S_{41}Se_{41}$	2.3764	2.3745	annealed
$As_{18}S_{41}Se_{41}$	2.3691	2.3673	not annealed

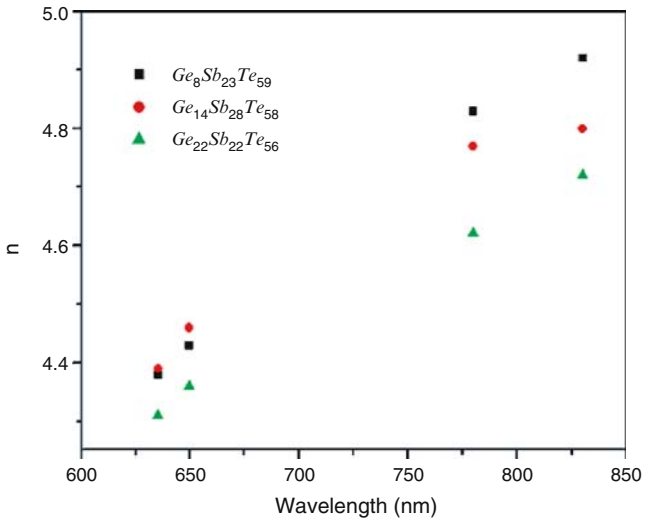

Fig. 1.7. Variation of refractive index n versus wavelength for $Ge_xSb_yTe_z$ films [89]

1.8 Photoinduced Changes in Chalcogenide Glasses

1.8.1 Photoinduced Phenomena

At least seven distinct photoinduced phenomena are exhibited by amorphous chalcogenides [90, 91]. These include photocrystallization or (amorphization),

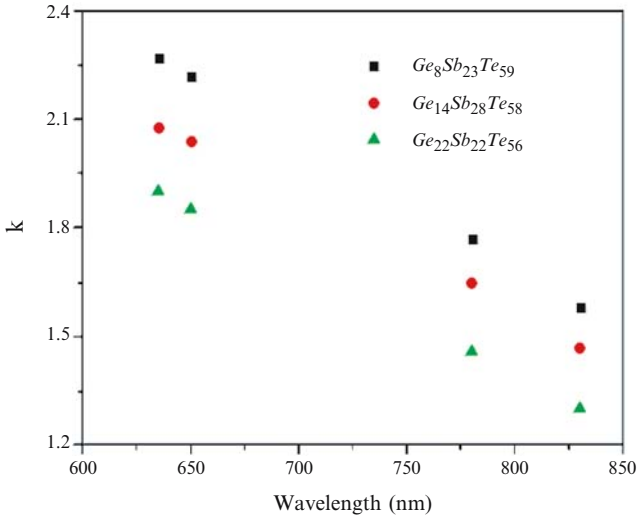

Fig. 1.8. Variation of extinction coefficient k versus wavelength for $Ge_xSb_yTe_z$ films [89]

photopolymerization, photodecomposition, photocontraction or expansion, photovaporization, photodissolution of metals such as Ag into the chalcogenide, and light-induced change in local atomic configuration. These changes are accompanied by changes in the optical constants, i.e., changes in the electronic band gap, refractive index and optical absorption coefficient. X-ray studies of volume expansion are shown in Fig. 1.9 [92]. We see in the upper pattern that the first sharp diffraction peak is located at a wavenumber-transfer value of $Q \sim 1.2\,\text{Å}^{-1}$. The lower curve shows the intensity difference between the annealed and illuminated states, with positive difference values indicating a decrease in the X-ray intensity with illumination. The results show that the peak intensity decreases with illumination. In addition, the peak broadens asymmetrically. This asymmetric change can be interpreted as a manifestation of interlayer cracking [92]. In distorted layer structures (as a result of illumination) with a typical interlayer distance of ∼0.5 nm, in a few places the interlayer distance becomes as wide as ∼1 nm.

These light-induced changes are favored in chalcogenide glasses due to their structural flexibility (low coordination of chalcogens) and also due to their high-lying lone-pair p states in the valence band. Annealing chalcogenide glasses can affect the photoinduced changes. In particular, irreversible effects occur in as-deposited films, while reversible effects occur in well-annealed films as well as bulk glasses. Changes in local atomic structure are observed on illumination with light having a photon energy near the optical band gap of the chalcogenide. Although light-induced effects can also be observed at longer wavelengths, they generally necessitate much higher intensities.

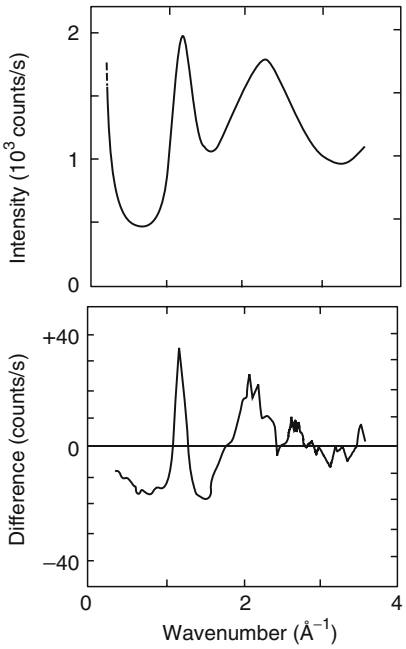

Fig. 1.9. An X-ray diffraction pattern of As_2S_3 glass (*top*) and the intensity change (*bottom*) induced by band gap illumination. A positive difference means an intensity reduction upon illumination (after [20, 92])

Photodarkening is sensitive to hydrostatic pressure, and it can be thermally erased by annealing near the glass-transition temperature. Photoinduced anisotropy (PA) is induced [3] when the glass or film is exposed to linearly polarized light and can be removed by exposure to unpolarized light or thermal annealing. When chalcogenide glasses are exposed to short laser pulses, large Kerr-type nonlinearities are induced. Photoinduced stable second-harmonic generation has also been reported in chalcogenide glasses [93]. These photoinduced effects can be used for the fabrication of devices such as gratings, waveguides, etc. (see Chaps. 1 and 7).

1.8.2 Exposure Characteristics

In order to explore the utility of photodarkening for device applications, a map of variation of intensity versus exposure for As_2S_3 films deposited by PLD has been measured [88]. Photodarkening was measured by monitoring the change in the transmission of a sample with time during illumination. Figure 1.10 shows a typical curve of transmissivity at 514.5 nm versus time. As is evident, the transmission of the sample decreases with time, approaching

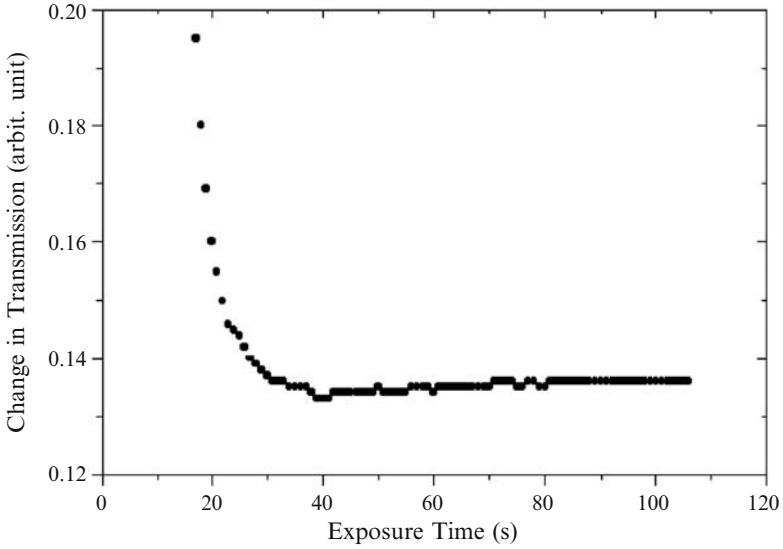

Fig. 1.10. Change of optical transmission of a 2 μm thick As_2S_3 film versus time during photodarkening at 514.5 nm. Illumination intensity of the green light was 30 mW mm^{-2}; the value 0.2 corresponds to 20% transmission (after [88])

a saturation point for long exposures. In order to see whether darkening is reversible or permanent, annealing at 150°C for 2 h under a nitrogen flow was performed after sample exposure. Annealing at this temperature allowed for maximum index change. It should be emphasized here that all the exposure measurements were obtained at a time for which maximum darkening had occurred (when the transmission of the sample had reached the saturation value). Figure 1.11 shows the result of intensity change versus exposure for As_2S_3 films [88]. As is seen, the exposure map divides into three distinctly different regions.

These results are very similar to those reported by the Laval group [94], although the latter films seem to be slightly less sensitive. This could be explained as partly due to a different composition of films used in [88] and partly to the fact that the films had been illuminated during the deposition in the PLD chamber. When using photodarkening to write waveguides using a laser, it is important to know the damage threshold corresponding to the intensity when the film starts to be ablated/melted off the substrate. This threshold was found to be $\approx 7,100$ mW mm^{-2} for PLD As_2S_3 films at 514.5 nm [88].

As a result, from Fig. 1.11 one can see that permanent photodarkening can be achieved at waveguide writing speeds of >100 μm s^{-1} at a subdamage irradiance of 5,600 mW mm^{-2}. On the basis of these results, Zakery [88] assembled a laser-writing system to fabricate channel waveguides about 3 μm wide. The

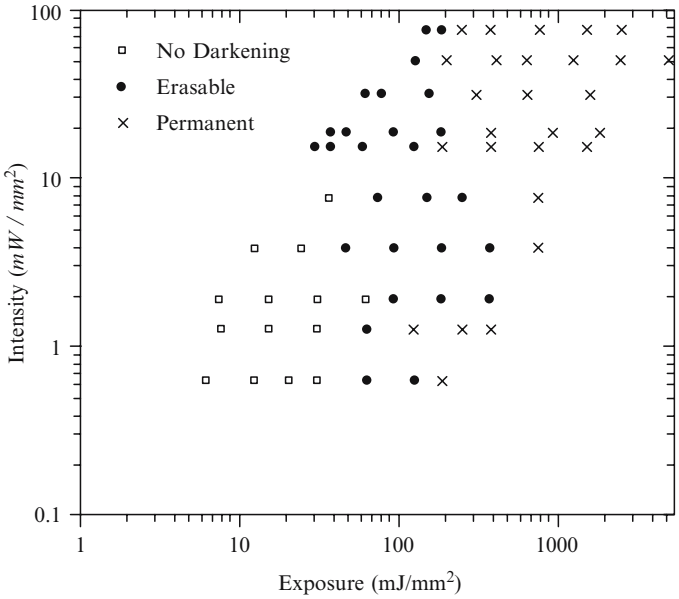

Fig. 1.11. Darkening map of films as a function of both intensity and exposure for a 4 µm thick sample irradiated at 514.5 nm with an argon laser and subsequently annealed at 150°C for 2 h [after 88]

514.5 nm green line of an argon laser was attenuated by passing through a neutral-density filter and then expanded by a pinhole. The expanded output was then focused on the sample using a 10× objective. PLD As_2S_3 films were deposited on a silicon wafer with an overlayer of 2.4 µm SiO_2. As-deposited As_2S_3 films with thicknesses up to 2 µm were used in which channel waveguides were fabricated.

1.8.3 Measurements of the Propagation Losses by a Prism Coupler

Measurements of waveguiding can be performed [88] using a prism coupler. An As_2S_3 film deposited with a SiO_2 overlayer, pressed against a high refractive-index prism ($n = 2.8659$ at 632.8 nm), can be rotated to find angular positions at which coupling into a waveguide mode is possible. It is possible to observe the propagation of guided light by detecting the light scattered from the sample with a CCD camera and the propagation loss can be calculated using the output intensity versus the propagation distance. The camera measured propagation distances of 4–5 cm at 632.8 nm. The results of loss measurements by the prism coupler are also shown in Fig. 1.12. The direct beam of an argon laser (green line) was used to expose an area of 5×1 cm on the sample and this

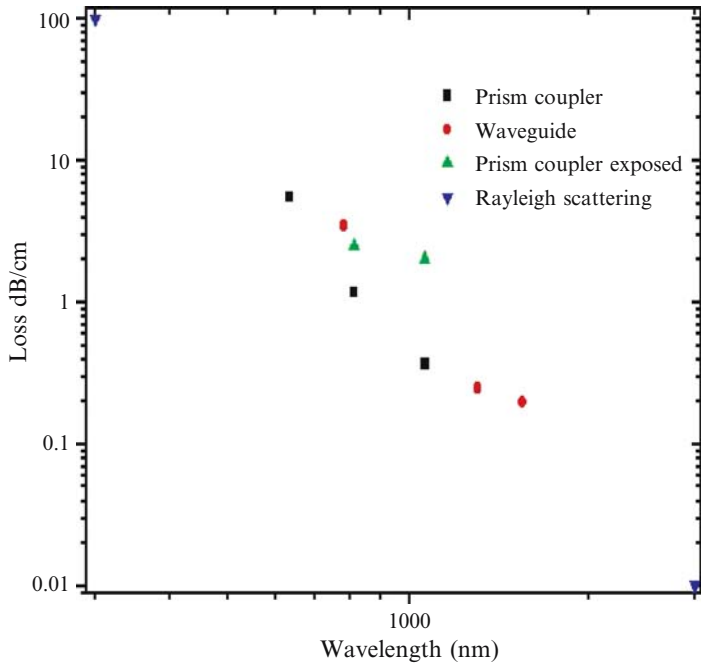

Fig. 1.12. Propagation loss versus wavelength for a 3 µm channel waveguide fabricated in PLD As_2S_3 films. Prism coupler corresponds to loss measurements using a prism-coupling technique described in the text, while waveguide corresponds to loss measurements in a fabricated waveguide. Prism-coupler exposed refers to the case where the sample was exposed prior to loss measurements (after [88])

exposed region was also used in propagation-loss measurements. Figure 1.12 shows losses of between 5 and 8 dB cm^{-1} measured at 632.8 nm.

Measured losses at 810 nm are between 1 and 2 dB cm^{-1}, while at 1,064 nm losses of between 0.3 and 0.7 dB cm^{-1} were measured for as-deposited films. For exposed samples, measured losses were between 1 and 2 dB cm^{-1} in the wavelength region of 780–1,064 nm [88].

1.8.4 Measurements of Propagation Losses in Laser-Written Waveguides

As_2S_3 films of up to 2 µm thickness were used for waveguide fabrication. Channel waveguides of 5 cm length and 3 µm width were written (using the direct laser writing set up described earlier) in these films. Light from different laser-diode sources at 780, 1,300, and 1,550 nm were used for these measurements. The output of the laser source was butt coupled to the film via a fiber of 5 µm diameter and the guided light through the waveguide was then coupled to a microscope objective and collected by a CCD camera. Figure 1.13 shows the

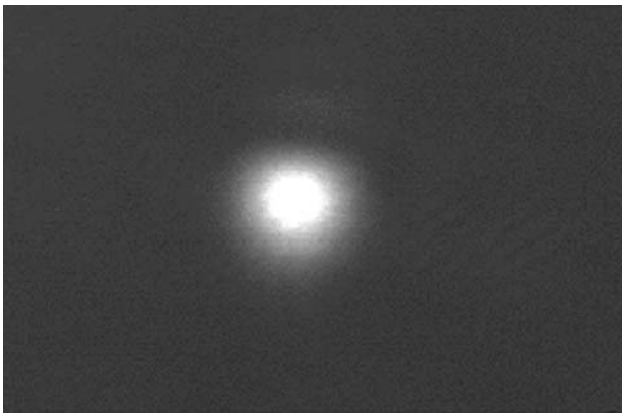

Fig. 1.13. Near-field image of the output of a single-mode photoinduced channel waveguide made in an As_2S_3 film measured at 780 nm (after [88])

near-field image of the output of a photoinduced channel waveguide written in these PLD films. Results of loss measurements for waveguides written in As_2S_3 films are also shown in Fig. 1.12. Losses lower than $0.3\,\mathrm{dB\,cm^{-1}}$ were measured at 1,550 nm.

1.9 Summary

Chalcogenide glasses are low-phonon-energy materials and are generally transparent from the visible to the infrared. Doping chalcogenide glasses by rare-earth elements has opened up numerous applications of active optical devices. Because of their large nonlinearities, chalcogenide glasses are promising candidates for AOS applications. The structure of chalcogenide glasses cannot be described by means of a continuous random network, but can be rather layer-like, as for example in As_2S_3, and chain-like, as in pure S or Se. Flexibility of their structures, as a result of the van der Waal's bonding between layers allows for easily accommodation of changes in their structures. Various structural techniques such as NIR Raman spectroscopy, RBS, WRS, and EXAFS have been used to probe different structural units present in chalcogenide glasses. Different techniques have been employed to determine the density of localized states in the gap and it is now generally believed that on top of a featureless distribution of states in the tails, a structured density of defect states exists, attributed to VAPs. It could be said that well-defined states exist in the gap of chalcogenide glasses. The absorption coefficient, α, of films has been measured using several techniques, such as with a conventional spectrophotometer in the visible region and PDS for wavelengths beyond the band edge. The results of PDS measurements have shown that as-deposited films have losses below $0.1\,\mathrm{dB\,cm^{-1}}$ across the telecommunica-

tion band. The optical gap obtained from the analysis of the data shows that chalcogenide glasses have optical gaps ∼2–3 eV. Various photoinduced effects, such as photodarkening, the metal-photodissolution effect and PA, have been used to fabricate devices such as gratings, waveguides, Bragg gratings, etc. Doping chalcogenide glasses with rare-earth elements has allowed the possibility of using these glasses for active applications such as amplifiers and lasers. Since chalcogenide glass fibers transmit in the IR, there are numerous potential applications in the civil, medical and military areas. Chalcogenide fibers are well-suited for chemical-sensor applications, such as fiber-optic chemical-sensor systems for quantitative remote detection and identification as well as detecting chemicals in mixtures. Different techniques have been used to measure the optical constants of chalcogenide glasses and films, such as optical transmission and reflection, ellipsometry, prism coupling, etc. While, up to now, evaporated and sputtered films have been used for producing films of chalcogenide glasses, pulsed laser-deposition of these films has proved useful. These PLD films have a stoichiometry similar to their parent materials and do not need annealing after deposition. They have been used in fabricating many devices, such as waveguides, fiber Bragg gratings, nonlinear directional couplers, etc. using light-induced photostructural changes. Results of loss measurements in laser-written waveguides show that losses lower than 0.3 dB cm^{-1} at 1,550 nm are found for a typical chalcogenide glass such as As_2S_3.

http://www.springer.com/978-3-540-71066-0

Optical Nonlinearities in Chalcogenide Glasses and their Applications

Zakery, A.; Elliott, S.R.

2007, IX, 202 p., Hardcover
ISBN: 978-3-540-71066-0